18

Confocal laser microscopy of photoinduced diffusion of $CsPbBr_3$ perovskite nanoplatelets and cubic-shaped nanocrystals

© L.N. Borodina, D.A. Tatarinov, K.I. Annas, V.N. Borisov, A.V. Veniaminov

International Research and Educational Center for Physics of Nanostructures, ITMO University, St. Petersburg, Russia

e-mail: lnborodina@itmo.ru

Received November 24, 2025
Revised November 24, 2025
Accepted December 01, 2025

The hydrodynamic size of cubic nanocrystals and rectangular nanoplatelets of $CsPbBr_3$ perovskite diffusing in a colloidal solution were determined using stripe-Fluorescence Recovery After Photobleaching (sFRAP) technique and compared with their geometric dimensions obtained by transmission electron microscopy. The edge lengths and volumes of the cubic nanocrystals and nanoplatelets differ by a factor of 1.5−2, but their measured hydrodynamic sizes are almost identical: 15 ± 5 nm and 13 ± 5 nm. Variations in the nanocrystal size within the ensemble manifest themselves in luminescence (sFRAP) measurements through the nonlinearity of the time dependence of the squared width of the photoinduced spatial inhomogeneity.

Keywords: perovskite quantum dots, nanoplatelets, diffusion of nonspherical nanoparticles, hydrodynamic size, confocal microscopy, Fluorescence Recovery after Photobleaching (FRAP).

DOI: 10.61011/EOS.2025.12.63189.8816-25

Introduction

Among the variety of today's photonics materials, perovskite nanocrystals (NC) and nanoplatelets (NP) are of special interest due to their outstanding optical properties, such as high photoluminescence (PL) quantum yield, significant single- and multiphoton absorption, high optical stability and defect tolerance, and bright narrowband PL in the entire visible spectral range. Combined with inexpensive and relatively simple methods for synthesizing perovskites, these properties make them ideal candidates for modern optoelectronics, photonics, and nonlinear optics devices [1–4]. Additionally, colloidal perovskite NC (quantum dots) and NP can be easily embedded in complex multicomponent systems by replacing ligands on their surfaces, thus making it possible to design and fabricate the new hybrid materials with unique optical properties and also use the perovskite nanostructures in biomedical applications [5–8].

Over the past decade, a large number of studies have been published shedding light on the photovoltaic properties, optical characteristics, and stability of $CsPbBr_3$perovskite NC and NP, however, their transport and hydrodynamic properties critical for many potential biomedical and technical applications, such as targeted delivery and formation of photonic structures from photoinduced diffusion, are still not properly studied. Among the key parameters determining the behavior of NC in colloidal solutions is the diffusion coefficient, which is closely related to their hydrodynamic sizes.

Conventional approaches imply the diffusion of spherical particles in a continuous medium, but perovskite particles have a noticeably non-spherical shape. It is not obvious how the mobility of NC or NP is related to the geometry of nanoparticles obtained by means of electron or atomic force microscopy, and, for example, the dynamic light scattering method is not applicable to colloidal solutions with a high concentration of nanoparticles. However, when creating diffractive, laser, and sensor structures by holographic recording in a photopolymerizable composition using photoinduced diffusion [9–12], the spatial redistribution of nanoparticles of various morphologies shall be taken into account.

The present paper outlines the experimental research of the photoinduced diffusion of cubic-shaped perovskite NC and rectangular NP by fluorescence recovery after photobleaching technique and the comparison of the revealed features with the nanocrystals geometry observed on electron microscopic images.

Materials and research methods

The following substances were used for the synthesis of NC and NP of perovskite: 1-octadecene (ODE, 90 %, Merck), oleic acid (OA, 90 %, Sigma-Aldrich), oleylamine (OlAm, 70 %, Sigma-Aldrich), cesium carbonate (Cs_2CO_3, 99.9 %, Sigma-Aldrich), lead bromide (II) ($PbBr_2$, $\geq$ 99.999 %, Sigma-Aldrich), toluene and hexane (Vecton), ethyl acetate (EtOAc, anhydrous, $\geq$ 99.5 %, Sigma-Aldrich).

To chemically synthesize NC and NP of the perovskite $CsPbBr_3$ the precursor of cesium oleate was prepared (Cs−OA). It was fabricated using the method in [13]: the appropriate amount of Cs_2CO_3, dehydrated oleic acid (OA)

and 1-octadecene (ODE) were placed into a 50 mL three-neck flask. The mixture was degassed at 120 °C for 30 min, after which it was heated in a nitrogen atmosphere to 150 °C until the solid phase was completely dissolved. Then the temperature was set to 120 °C and maintained until the injection of Cs–OA.

The NC of $CsPbBr_3$ were synthesized with some modifications of the method published in [13]. $PbBr_2$, dried OA and OlAm, as well ODE were placed into a 50 mL three-neck flask. The mixture was degassed under vacuum at 120 °C for 30 min, and then transferred to a nitrogen atmosphere. After complete dissolution of salt, the temperature was increased to 180 °C and a hot solution of Cs–OA was quickly introduced. After 5 s, the reaction was stopped by cooling in an ice bath. The obtained nanocrystals were precipitated by centrifugation (6000 min^{-1}, 10 min), washed with ethyl acetate (1:2 hexane:ethyl acetate), precipitated again and resuspended in hexane. Additional centrifugation at a speed of 3000 min^{-1} made it possible to separate the filler fraction with purified nanocrystals of $CsPbBr_3$.

The nanoplatelets of $CsPbBr_3$ were synthesized using method described in [14]. $PbBr_2$, OA, OlAm, and ODE were added to a separate three-necked flask, after which the mixture was degassed at 120 °C for 20 min and the process was continued in nitrogen. After complete dissolution of the reagents, the temperature was lowered to 25 °C and a pre-prepared Cs–OA solution was quickly introduced. The reaction mixture was then heated to 180 °C and the reaction was immediately stopped by cooling in the ice bath. The formed NP was purified by centrifugation: first at 6000 min^{-1} for 5 min, then it was redeposited, dispersed in hexane and re-centrifuged at 3000 min^{-1} to isolate the additive fraction containing purified nanoplatelets of $CsPbBr_3$.

The spectra of optical absorption and PL of the synthesized NC and NP of perovskite $CsPbBr_3$ (Fig. 1, *a, b*) were recorded using spectrophotometer UV-3600 (Shimadzu, Kyoto, Japan) and spectrofluorometer Panorama (Lumex, Saint-Petersburg, Russia).

The nanocrystals of $CsPbBr_3$ are characterized by a pronounced exciton absorption band with a maximum at 500 nm and by PL maximum at 510 nm when excited by radiation with a wavelength of 405 nm (Fig. 1, *a*). The full width at half maximum (FWHM) of PL spectrum makes 21 nm which is an evidence of the high degree of uniformity of the ensemble.

The nanoplatelets of $CsPbBr_3$ demonstrate a more short-wave exciton absorption band with a maximum at 444 nm (Fig. 1, *b*). The PL maximum at 405 nm excitation is observed at a wavelength of 454 nm, while FWHM is 19 nm, which also indicates the high spectral purity of the samples. Both types of nanostructures are characterized by high photostability.

The quantum yield of PL, determined relative to Rhodamine 6G in ethanol as the reference, was 74% for NC and 21% for NP.

Electron microscopic images of NC (Fig. 1, *c*) and NP (Fig. 1, *d*) were obtained by transmission electron microscopy (TEM) using microscope JEOL JEM-1011 (JEOL, Tokyo, Japan). To prepare the samples, stock solutions of NC and NP were pre-diluted approximately 50-fold, after which a small amount of the diluted solution was applied to copper grids with a carbon substrate and dried in air.

TEM-images of NC demonstrate primarily a cubic morphology of particles with the edge length of 8–11 nm (Fig. 1, *e*) which is characteristic for $CsPbBr_3$ NCs synthesized by hot injection method. TEM-images of NP (Fig. 1, *d*) show the rectangular platelets with the length of edges 21–30 nm and 14–27 nm (Fig. 1, *f, h*) and thickness of 2.5 nm. Ordered stacks of NP are also visible, oriented edge-on to the observer, which is typical for two-dimensional perovskite nanostructures.

The nanocrystals' average hydrodynamic size, as measured by Dynamic Light Scattering (DLS) using Zetasizer Nano ZS analyzer (Malvern Panalytical, Great Britain), was 11.9 ± 2.7 nm (Fig. 1, *g*), in consistency with the sizes obtained from the TEM analysis.

Luminescence-microscopic study of diffusion

The study of diffusion by method of Fluorescence Recovery After Photobleaching (FRAP) [15–18] consists in changing the photoluminescence (PL) efficiency in a certain area of the sample exposed to light and further monitoring the change in PL intensity due to photoinduced diffusion — a spatial redistribution of particles with modified and initial PL efficiency initiated by light impact. The use of FRAP method with the laser scanning microscopy has made it a way more flexible due to the formation of optical inhomogeneities of arbitrary shape in the studied sample and due to the analysis of not only the integral intensity of PL, but also its intensity distribution in space.

In this paper, we use sFRAP (*Stripe*-FRAP) [19] method based on recording a narrow stripe in an object with a focused laser beam and analyzing the PL intensity distribution in the direction perpendicular to the stripe due to diffusion. Information about diffusion can be obtained from the evolution of PL spatial profile width.

This approach allows us to consider diffusion as one-dimensional, and take into account the particles drift, changes in PL intensity during image construction after exposure, and photoinduced changes in the particles diffusivity. sFRAP experiments were performed using confocal laser scanning microscope LSM 710 (Carl Zeiss, Germany). To carry out measurements, a 1 mm thick cuvette with as-synthesized stock colloidal solution of perovskite nanoparticles (NC or NP) was placed horizontally on a microscope stage and the radiation of a diode laser with a wavelength of 405 nm was focused into it using objective lenses with magnification 10× or 20× and a numerical aperture

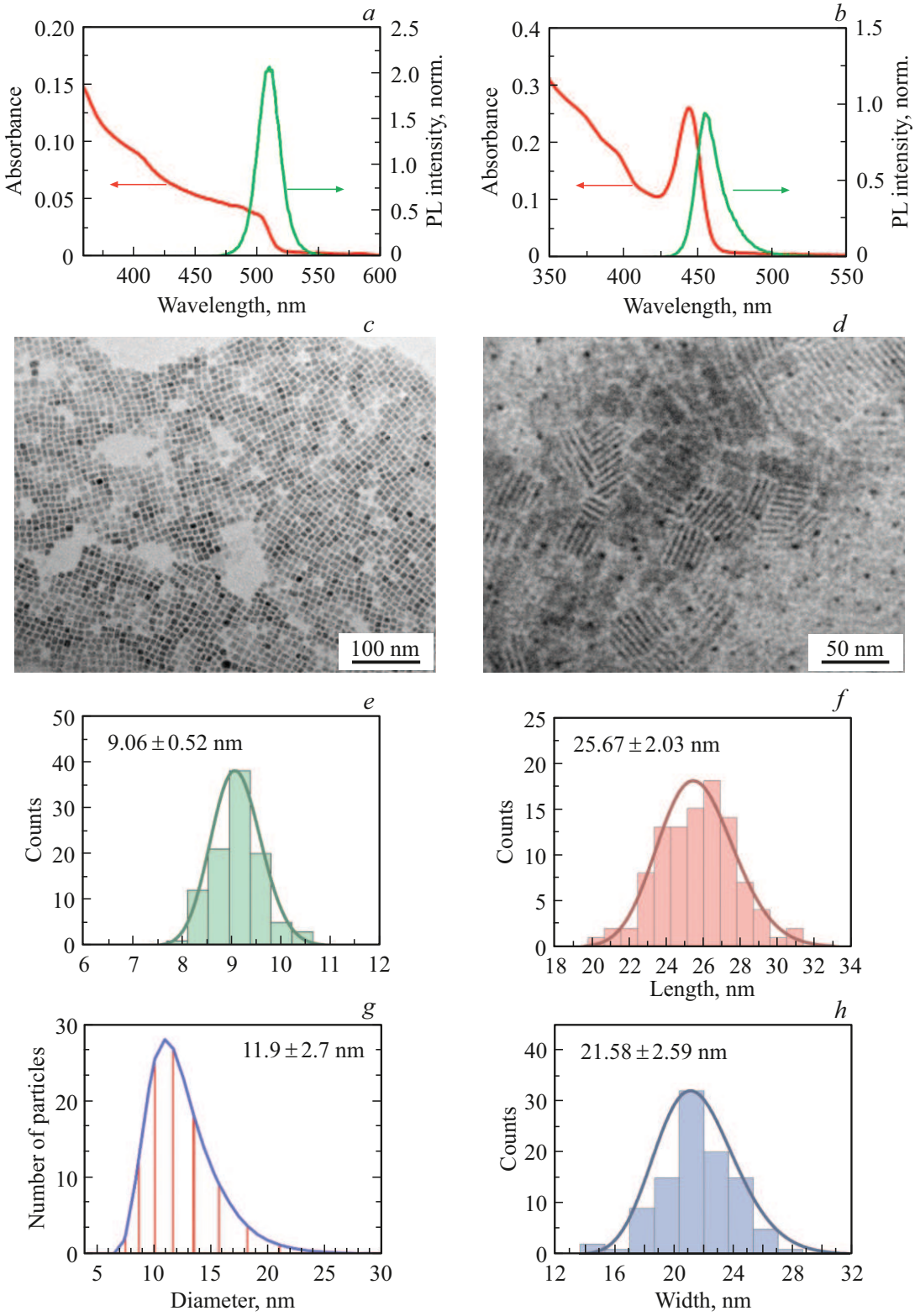

Figure 1. Absorption spectra (red lines) and PL spectra upon excitation with 405 nm radiation (green lines) of cubic NC (*a*) and NP (*b*), electron microscopic images of NC and NP (respectively *c* and *d*) and associated histograms of distribution along the length of NC edge (*e*), along the length and width of NP (*f* and *h*) size distribution of NC according to dynamic light scattering (DLS) data (*g*).

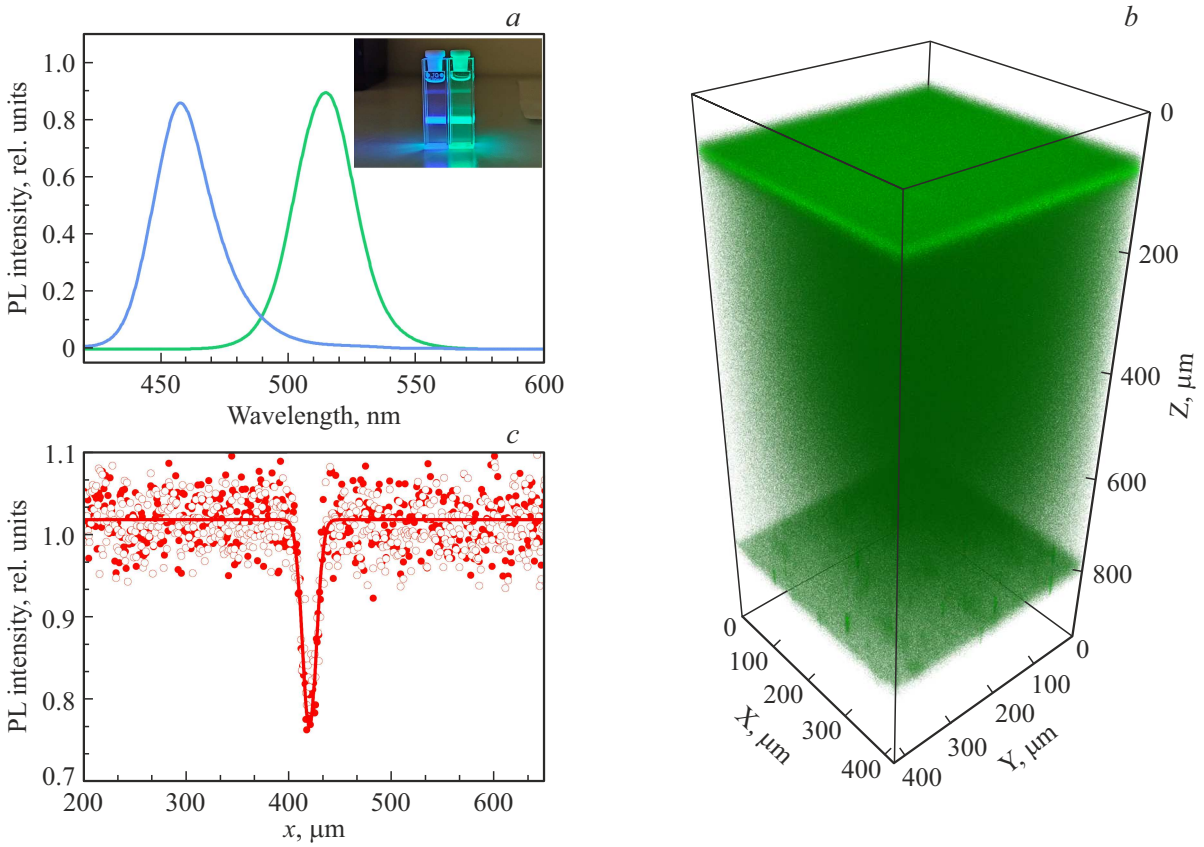

Figure 2. PL spectra of nanoplatelets (blue curve) and nanocrystals (green curve) of $CsPbBr_3$ perovskites measured using a laser scanning microscope when excited by laser radiation with a wavelength of 405 nm (the inset illustrates the luminescent colloidal solutions of perovskite NP and NC in cuvettes at the same excitation wavelength) (*a*). Cuvette surface effect: volumetric distribution of the luminescence intensity of a colloidal solution of perovskite NP under excitation radiation incident from above (increased PL intensity is observed on the inner surfaces of the cuvette glasses) (*b*) and PL profiles in the direction transverse to the exposed stripe, recorded 1 s and 50 s (dark and light dots) after exposure (profile width is unchanged and makes 14 μm) (*c*).

of 0.2 or 0.4, respectively. Such numerical apertures are a compromise between the efforts to avoid high beam divergence (of different widths of the exposed stripe at different depths) and to reduce the thickness of the layer from which the detected PL is collected—*optical slice thickness* in order to meet the one-dimensional diffusion approximation. Size of the scanned area from 400×400 to $1400 \times 1400\,\mu$m, width of the scanned area $20\,\mu$m. PL intensity was detected by the photodetectors in the spectral ranges corresponding to the PL bands of NC and NP (Fig. 2, *a*).

Three-dimensional scanning of the colloidal solution inside the cuvette shows that its PL intensity is unevenly distributed in the volume (Fig. 2, *b*). In addition to PL attenuation with depth due to the absorption of excitation radiation, there is an increased intensity of PL on the inner surfaces of the cuvette, which indicates the adsorption of nanoparticles on them. The adsorbed nanoparticles can retain the ability to photo-transformation, but not to diffusion, and in sFRAP experiment, when focusing laser radiation on the surface, the exposed band remains unchanged (Fig. 2, *c*). Therefore, to study the diffusion of nanoparticles in a solution, its volume is needed that is separated from the surface by a certain distance, but not too large, so that the intensity of the excitation radiation remains sufficient. In this study, the distance $100\,\mu$m is selected for the optical slice thickness $10-20\,\mu$m, set by the numerical aperture of the lens and the diameter of the confocal aperture.

The analysis of the change in spatial distribution of PL intensity in the direction transverse to the photo-transformed stripe makes it possible to determine the diffusion coefficient of nanoparticles by the rate of change in the band width, and then calculate the apparent hydrodynamic diameters of the nanoparticles. To determine the stripe width, in the simplest but fairly typical case the PL intensity profile is approximated by the Gaussian function, which is the fundamental solution to the diffusion equation at a constant coefficient. In this case, the squared width of the Gaussian profile depends linearly on time, and the diffusion coefficient is determined by the slope: $D = \Delta w^2/8\Delta t$.

However, e.g., if the diffusivity of nanoparticles changes as a result of exposure, the PL profile is described not by a

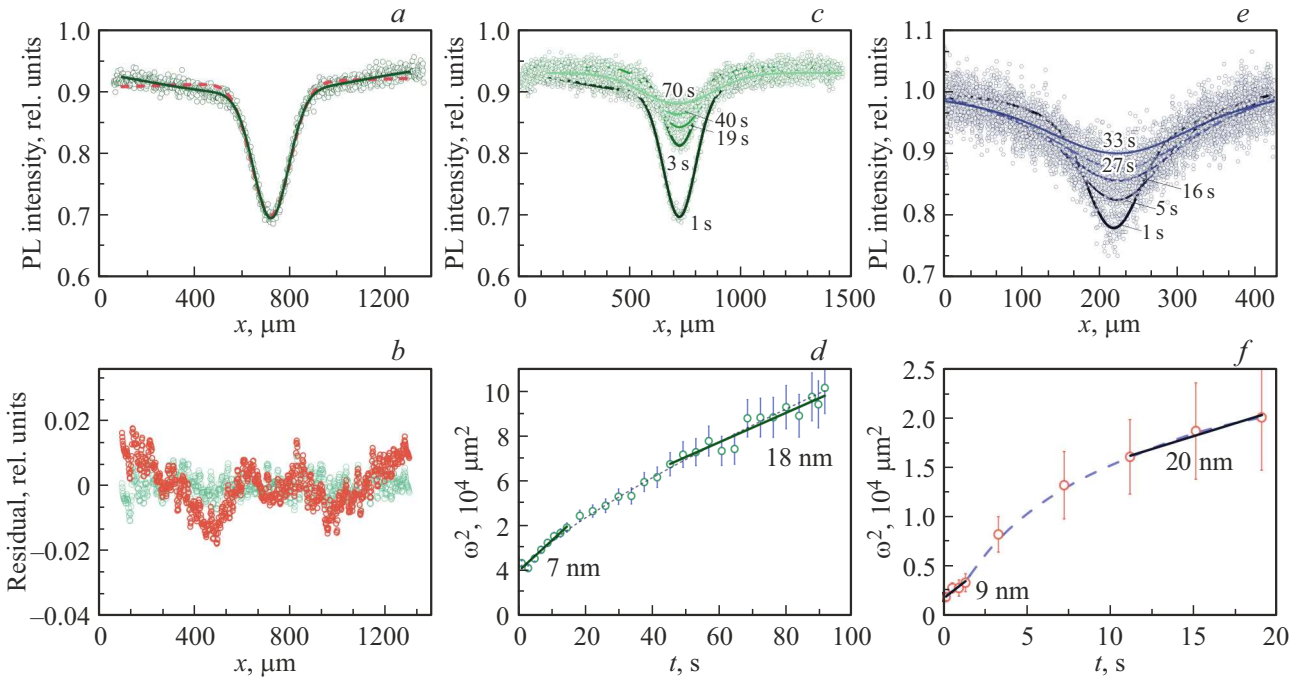

Figure 3. Results of the perovskite NC and NP study by sFRAP: *a* — PL profile of NC in the direction perpendicular to the exposed stripe and the result of its approximation Gaussian function(orange dashed curve) and by the sum of two Gaussian functions (solid green curve); *b* — the corresponding residuals; PL spatial profiles of cubic NC, measured at various time intervals after exposure (*c*) and the corresponding squared profile width versus time (*d*), approximated by a power function for ease of perception and by straight lines for determining apparent hydrodynamic diameters, which are also indicated on the graph; similar sequences of PL profiles (*e*) and the quared profile width versus time (*f*) for the nanoplatelets.

single Gaussian function, but by the difference of two such functions with different rates of their broadening [19].

The PL profiles of NC also demonstrated a deviation from the Gaussian shape immediately after exposure. The optimal approximation by the sum of two Gaussian functions (Fig. 3, *a, b*) indicates not a change in the diffusion coefficient under the action of light, but the initial presence of two diffusing components in the colloidal solution, similar to what was noted in studies on the diffusion of a model system of luminescent polystyrene spheres of various diameters [20]. One of the Gaussian components rapidly expands and goes beyond the scanned area, ceasing to contribute to the PL profiles: within a few seconds after exposure, they approach a Gaussian shape (Fig. 3, *c*). The dependence of PL profile squared width on time, shown in Fig. 3, *d*, turns out to be nonlinear. This corresponds to the presence of diffusing nanocrystals of perovskites of various sizes in the ensemble (Fig. 1, *c, e*). According to the curve's slope at various times, the range of hydrodynamic diameters of NC is estimated as 7−18 nm, in good agreement with the results obtained by dynamic light scattering (7−23 nm, Fig. 1, *g*).

The dependence of the squared width of PL profile of NP on time, obtained from the analysis of the sequence of PL profiles (Fig. 3, *e*), is also nonlinear (Fig. 3, *f*). The change in its slope indicates the presence of NP in the ensemble with apparent hydrodynamic diameters in the range from 9 to 20nm, which almost coincides with the range of hydrodynamic sizes of NC, despite the significant difference in the edge lengths of these nanoparticles: 8−11 nm for NC (Fig. 1, *e*) against 16−30 nm for NP (Fig. 1, *f, h*) and their volumes: respectively 500−1300 nm^3 against 800−2100 nm^3.

Data on the translational diffusion of particles in a colloidal solution, assuming their spherical shape, are interpreted using Stokes-Einstein equation, which relates the diffusion coefficient to the diameter of a particle:

$$D = \frac{k_B T}{6\pi\eta r}.$$

To apply this equation to non-spherical particles, it is required to determine their size in a reasonable way. The natural spatial scale of a cube is the length of its edge a. But the cube is obviously larger than the sphere with a diameter equal to the length of its edge — this is the size of the sphere inscribed in the cube, and diffuses slower. A sphere with a diameter equal to the spatial diagonal of a cube $\sqrt{3}a$, circumscribed around the cube, is large in comparison with it. The authors of [21] have shown that the force of hydrodynamic friction of a cubic particle is close to the force of friction of a sphere, whose diameter is equal to the arithmetic mean between the diameters of the spheres inscribed in the cube and circumscribed around the cube $(\sqrt{3}+1)a/2$. This value can be taken as the calculated

hydrodynamic size of the cube, however, neglecting the solvate shell and ligands surrounding the real nanoparticle. The volume of such a sphere is several percent larger than the volume of the corresponding cube. This means, in particular, that with equal volumes, the cube experiences stronger hydrodynamic friction and diffuses slower than the sphere. The range of hydrodynamic diameters of cubic nanocrystals 7−18 nm measured by sFRAP method covers the range of sizes 10−14 nm calculated within the given rules for cubic NC with the edges of 8−11 nm observed using the electron microscopic images (Fig. 1, *c, e*), and the average sizes are equal.

To consider the hydrodynamic properties of plate-shaped diffusing particles, it is convenient to use a thin disk into which, in the limit of an infinite ratio of two long axes to a short one, an oblate spheroid is transformed. The hydrodynamic friction force of a thin disk with a radius of R, averaged over its various orientations, is equal $f = 12\eta R$ [22], and the equivalent radius of a sphere experiencing the same solvent resistance during translational diffusion (Stokes radius) — $2R/\pi$. The authors of [23] calculate the friction force of a plate of arbitrary shape through the friction force of a disk of the same area, multiplying it by an expression linear in the thickness of the disk, but weakly dependent on it. For a square or near-square rectangular plate with an area S with edges $\approx \sqrt{S}$ and thickness h the friction force during diffusion in a medium with viscosity η makes $f = 12\eta(1.035\sqrt{S/\pi} + 0.68h)$, while the Stokes radius is — $2/\pi(1.035\sqrt{S\pi} + 0.68h)$. According to these concepts, the calculated hydrodynamic diameter of a nanoplate with ensemble-average sizes of $25.7 \times 21.6 \times 2.5$ nm will be 20 nm. The NP effective sizes determined by sFRAP method were found to be in the range from 9 to 20 nm (Fig. 3,*f*), slightly lagging behind the values of 15−24 nm calculated from the NP geometry (Fig. 1, *d,f*), although the hydrodynamic sizes obtained from experimental data on diffusion would be expected to exceed the values found by the electron microscopy. One of the reasons for this discrepancy may be the small size of NP sampling used as the basis for estimating their geometry.

Conclusion

In this study covering the specifics of diffusion of colloidal perovskite nanocrystals of various shapes in experiments with light-induced luminescence inhomogeneities, a similar diffusion behavior of cubic nanocrystals with flat rectangular nanoplatelets was found, exceeding them by 1.5−2 times in linear sizes and volume. The presence of nanoparticles of various sizes in the ensemble, which can be observed in the electron microscopic images, is manifested in the luminescence microscopic experiments as a nonlinearity of the luminescence intensity profile square width versus time. Estimates of the hydrodynamic sizes of cubic nanocrystals based on their geometric dimensions are close to the results of optical measurements, and for the nanoplatelets they give slightly overestimated values.

Funding

The research was carried out with the financial support of the Russian Science Foundation, project № 25-23-00708 „Photoinduced diffusion of perovskite quantum dots based on laser microscopy and holographic relaxometry for photonics diffraction devices“, https://rscf.ru/project/25-23-00708/.

Conflict of interest

The authors declare that they have no conflict of interest.

References

[1] D. Tatarinov, A.O. Ismagilov, A.V. Koroleva, E. Zhizhin, W. Zheng, A.V. Baranov, A.P. Litvin. Nanoscale, **17**, 6695–6703 (2025). DOI: 10.1039/D4NR05049E

[2] D.A. Tatarinov, J. Xie, Q. Qian, Q. Wang, N.A. Maslova, L.N. Borodina, A.P. Litvin, H. Huang. Chin. J. Chem., **42**, 2779–2787 (2024). DOI: 10.1002/cjoc.202400513

[3] A.P. Litvin, J. Guo, J. Wang, X. Zhang, W. Zheng, A.L. Rogach. Small, **21**, 2408422 (2025). DOI: 10.1002/smll.202408422

[4] Z. Liu, X. Qin, Q. Chen, T. Jiang, Q. Chen, X. Liu. Advanced Materials, **35**, 2209279 (2023). DOI: 10.1002/adma.202209279

[5] S. Wang, A.A. Yousefi Amin, L. Wu, M. Cao, Q. Zhang, T. Ameri. Small Struct., **2**, 2000124 (2021). DOI: 10.1002/sstr.202000124

[6] W. Lv, L. Li, M. Xu, J. Hong, X. Tang, L. Xu, Y. Wu, R. Zhu, R. Chen, W. Huang. Advanced Materials, **31**, 1900682 (2019). DOI: 10.1002/adma.201900682

[7] K. Sakhatskyi, A. Bhardwaj, G.J. Matt, S. Yakunin, M.V. Kovalenko. Advanced Materials, **37**, 2418465 (2025). DOI: 10.1002/adma.202418465

[8] Y. Shi, X. Deng, Y. Gan, L. Xu, Q. Zhang, Q. Xiong. Advanced Materials, **37**, 2413559 (2025). DOI: 10.1002/adma.202413559

[9] J.T. Sheridan, R.K. Kostuk, A.F. Gil, Y. Wang, W. Lu, H. Zhong, Y. Tomita, C. Neipp, J. Rancés, S. Gallego, I. Pascual, V. Marinova, S.H. Lin, K.Y. Hsu, F. Bruder, S. Hansen, C. Manecke, R. Meisenheimer, C. Rewitz, T. Rölle, S. Odinokov, O. Matoba, M. Kumar, X. Quan, Y. Awatsuji, P.W. Wachulak, A.V. Gorelaya, A.A. Sevryugin, E.V. Shalymov, V.Yu. Venediktov, R. Chmelik, M.A. Ferrara, G. Coppola, A. Márquez, A. Beléndez, W. Yang, R. Yuste, A. Bianco, A. Zanutta, C. Falldorf, J.J. Healy, X. Fan, B.M. Hennelly, I. Zhurminsky, M. Schnieper, R. Ferrini, S. Fricke, G. Situ, H. Wang, A.S. Abdurashitov, V.V. Tuchin, N.V. Petrov, T. Nomura, D.R. Morim, K. Saravanamuttu. Journal of Optics (United Kingdom), **22**, 123002 (2020). DOI: 10.1088/2040-8986/abb3a4

[10] Y. Tomita, E. Hata, K. Momose, S. Takayama, X. Liu, K. Chikama, J. Klepp, C. Pruner, M. Fally. J. Modern Optics, **63**, S1–S31 (2016). DOI: 10.1080/09500340.2016.1143534

[11] T.N. Smirnova, O.V. Sakhno, P.V. Yezhov, L.M. Kokhtych, L.M. Goldenberg, J. Stumpe. Nanotechnology, **20**, 245707 (2009). DOI: 10.1088/0957-4484/20/24/245707
[12] L. Borodina, V. Borisov, K. Annas, A. Dubavik, A. Veniaminov, A. Orlova. Materials, **15**, 8195 (2022). DOI: 10.3390/ma15228195
[13] L. Protesescu, S. Yakunin, M.I. Bodnarchuk, F. Krieg, R. Caputo, C.H. Hendon, R.X. Yang, A. Walsh, M.V. Kovalenko. Nano Lett., **15**, 3692–3696 (2015). DOI: 10.1021/nl5048779
[14] D. Yang, Y. Zou, P. Li, Q. Liu, L. Wu, H. Hu, Y. Xu, B. Sun, Q. Zhang, S.T. Lee. Nano Energy, **47**, 235–242 (2018). DOI: 10.1016/j.nanoen.2018.03.019
[15] P.S. Russo, J. Qiu, N. Edwin, Y.W. Choi, G.J. Doucet, D. Sohn. *Soft Matter Characterization*, ed. by R. Borsali, R. Pecora (Springer, 2008) p. 605–636. DOI: 10.1007/978-1-4020-4465-6_10
[16] D. Dey, S. Marciano, A. Nunes-Alves, V. Kiss, R.C. Wade, G. Schreiber. J. Mol. Biol., **433**, 166898 (2021). DOI: 10.1016/j.jmb.2021.166898
[17] N. Lorén, J. Hagman, J.K. Jonasson, H. Deschout, D. Bernin, F. Cella-Zanacchi, A. Diaspro, J.G. McNally, M. Ameloot, N. Smisdom, M. Nydén, A.M. Hermansson, M. Rudemo, K. Braeckmans. Q. Rev. Biophys., **48**, 323–387 (2015). DOI: 10.1017/S0033583515000013
[18] M. Carnell, A. Macmillan, R. Whan. *Methods in Molecular Biology*, ed. by Dylan M. Owen, (Humana Press Inc., 2015) p. 255–271. DOI: 10.1007/978-1-4939-1752-5_18
[19] L.N. Borodina, V.N. Borisov, A.V. Veniaminov. Opt. Spectrosc., **132** (9), 914–923 (2024). DOI: 10.61011/EOS.2024.09.60046.6730-24
[20] G.I. Hauser, S. Seiffert, W. Oppermann. J. Microsc., **230**, 353–362 (2008). DOI: 10.1111/j.1365-2818.2008.01993.x
[21] K. Okada, A. Satoh. Mol. Phys., **118**, 1–13 (2020). DOI: 10.1080/00268976.2019.1631498
[22] B.R. Jennings, K. Parslow. Proc. R. Soc. Lond. A, **419**, 137–149 (1988). DOI: 10.1098/rspa.1988.0100
[23] J.G. Hernández-Cifre, R. Rodríguez-Schmidt, C.M. Almagro-Gómez, J. García de la Torre. Polymer, **262**, 125467 (2022). DOI: 10.1016/j.polymer.2022.125467

Translated by J.Savelyeva